Solution structure of the transmembrane domain of the insulin receptor in detergent micelles

CrossMark

Qingxin Li [a], Ying Lei Wong [b], CongBao Kang [b],*

[a] Institute of Chemical & Engineering Sciences, Agency for Science, Technology and Research (A*STAR), Singapore, Singapore
[b] Experimental Therapeutics Centre, Agency for Science, Technology and Research (A*STAR), Singapore 138669 Singapore

ABSTRACT

The insulin receptor (IR) binds insulin and plays important roles in glucose homeostasis by regulating the tyrosine kinase activity at its C-terminus. Its transmembrane domain (TMD) is shown to be important for transferring conformational changes induced by insulin across the cell membrane to regulate kinase activity. In this study, a construct $IR_{940-988}$ containing the TMD was expressed and purified for structural studies. Its solution structure in dodecylphosphocholine (DPC) micelles was determined. The sequence containing residues L962 to Y976 of the TMD of the IR in micelles adopts a well-defined helical structure with a kink formed by glycine and proline residues present at its N-terminus, which might be important for its function. Paramagnetic relaxation enhancement (PRE) and relaxation experimental results suggest that residues following the TMD are flexible and expose to aqueous solution. Although purified $IR_{940-988}$ in micelles existed mainly as a monomeric form verified by gel filtration and relaxation analysis, cross-linking study suggests that it may form a dimer or oligomers under micelle conditions.

© 2014 Elsevier B.V. All rights reserved.

1. Introduction

The insulin receptor (IR) belongs to receptor tyrosine kinase (RTK) family that contains single-pass transmembrane proteins and comprises 59 members in human [1,2]. RTK family protein interacts with its ligand to play critical roles in cellular signaling through regulating its kinase activity that phosphorylates specific tyrosine residues on other signaling proteins or itself [1,2]. The IR plays a critical role in regulation of glucose homeostasis through interacting with insulin [1,3]. Unlike other RTKs, the IR is a heterodimeric disulfide-linked protein composed of two α-subunits and β-subunits in the absence of its ligand [3]. Both α- and β-subunits are resulting from the cleavage of a same prorecceptor. The IR is encoded by its gene and transcribed into IR-A and B isoforms with 12 amino acids difference in the α-subunit [3]. The α-subunits are located outside of the cell membrane and contain two leucine-rich repeats (L1 and L2), a cysteine rich region (CR), and two fibronectin type III domains (FnIII1-2) [3,4]. The FnIII-2 contains a 120 amino acids insert (ID) with a protease cleavage site to generate the α and β subunits [1]. The β-subunits contain two FnIIIs, a transmembrane domain (TMD) and a tyrosine kinase catalytic domain that can be activated through ligand binding to the α subunits [4].

The effect of insulin on the structure of its receptor has been studied for many years. The possible mechanism of insulin induced receptor activation is that insulin binding to the IR induces conformational changes that can be transmitted to the cytoplasmic domain to facilitate its phosphorylation. Phosphorylation on tyrosine residues in the cytoplasmic domains creates docking sites for molecular interaction with downstream signaling proteins or stimulates its catalytic activity [5,6]. Structural studies have been conducted for the domains of the IR using different techniques including X-ray crystallography, NMR spectroscopy and dark-field scanning transmission electron microscopy [4,7,8]. Although structural study of the IR ectodomain is challenging due to its large size, flexibility, glycosylation and existence of disulfide bonds, structural studies have shown the structural basis for its interaction with insulin [4,7,9–12]. Structural basis for the two surfaces of insulin interacting with the IR domains has been provided by several studies [10,13,14]. It is evident that insulin binding to its receptor causes structural changes, but the precise effect of the conformational changes on the kinase domain still remains unresolved [6].

The TMD of the insulin receptor is within the β-subunit and contains 23 amino acids [15]. Earlier studies suggested that modification in the TMD could alter receptor internalization and insulin signaling [16,17]. Mutations in the TMD were shown to have effects on receptor biosynthetic processing and kinase activation [18]. Substitution of the entire TMD of the IR with the TMD of c-neu/erbB2 resulted in constitutive kinase activation in vitro, while replacing the TMD with that of glycophorin A inhibited insulin action [15]. Although the TMD of IR does not interact with insulin directly, studies have suggested that the TM–TM interactions may affect the activation of the kinase domain of the receptor [15].

The structure of the TMD of the IR was predicted to be an α-helix. There is no structure of this domain that has been reported so far. In

* Corresponding author at: 31 Biopolis Way, Nanos, #03-01, Singapore 138669, Singapore. Tel.: +65 64070602; fax: +65 64788768.
E-mail address: cbkang@etc.a-star.edu.sg (C. Kang).

this study, we purified a construct $IR_{940-988}$ containing the TMD and conducted structural studies in detergent micelles using NMR spectroscopy. Our results show that the TMD contains a helix and a kink when it is purified in DPC micelles. The residues 942–948 preceding the TMD have a propensity to be a short helix and may interact with membrane. Our cross-linking study suggested that it may form a dimer or oligomers under micelle conditions.

2. Materials and methods

2.1. Materials

The DNA polymerase, restriction enzyme for molecular cloning was purchased from New England Biolabs. The pET-29b plasmids were purchased from Merck. The SDS-PAGE system, NuPAGE® gels, DH5α competent cells and SDS-PAGE molecular weight standard were purchased from Invitrogen and Bio-rad. The Bl21 (DE3) competent cells for protein expression were purchased from StrataGen. β-D-1-thiogalactopyranoside (IPTG) and dithiothreitol (DTT) and detergents were purchased from Anatrace or Avanti. The $^{15}NH_4Cl$, ^{13}C-glucose and D_2O were purchased from Cambridge Isotope. All other chemicals were purchased from Sigma.

2.2. Expression and purification of TMD of IR

The cDNA encoding residues Thr940 to Leu988 ($IR_{940-988}$) of human IR were synthesized (Genscript). Sequence number is based on the sequence from the protein knowledgebase (www.uniprot.org) with access number P06213. The cDNA was cloned into the NdeI and XhoI sites of pET29b to generate a plasmid-pET29-IRTM encoding a protein sequence with extra residues (EHHHHHH) at its C-terminus to aid protein purification. The resulting plasmid was transformed in *Escherichia coli* (*E. coli*) competent cells and plated onto LB plates containing kanamycin. Two to three colonies were picked up and inoculated in 10 ml of M9 medium and cultured at 37 °C overnight. The overnight culture was then inoculated into 1 l M9 medium with antibiotics. When OD_{600} reaches 0.6–1.0, protein was induced for 12 h at 37 °C by adding IPTG to 1 mM. Isotope-labeled proteins were also induced using the similar method except using labeled carbon and nitrogen sources [19]. The *E. coli* cells were harvested by centrifuging at 11,000 ×g for 10 min at 4 °C, and the cell pellets were re-suspended into a lysis buffer (20 mM Tris-HCl, pH 7.8, 300 mM NaCl, and 2 mM β-mercaptoethanol) and were then broken up by sonication on ice. The cell lysate was cleared by centrifugation at 20,000 ×g for 20 min. The pellet was washed with the lysis buffer one time and collected with centrifugation to obtain inclusion bodies. Inclusion bodies were solubilized in a urea buffer (8 M urea, 300 mM NaCl, 7 mM SDS, 20 mM Tris-HCl, pH7.8) by rotating at room temperature for 2–10 h [20,21]. The solution was then cleared by centrifugation at 48,000 ×g for 20 min at room temperature. The supernatant was loaded in a gravity column containing nitrilotriacetic acid saturated with nickel (Ni^{2+}-NTA) resin. Next, the resin was washed with 10 column volumes of urea buffer. Urea was then removed by washing resin with 10 column volumes of lysis buffer with 7 mM SDS and 20 mM imidazole. Protein was eluted with an elution buffer (300 mM imidazole, pH6.5, 2–20 mM detergent) after washing resin with 10 column volumes of washing buffer (lysis buffer with 2–20 mM detergent). To prepare an NMR sample that is selectively labeled with a ^{15}N-labeled amino acid, the Bl21 (DE3) *E. coli* cells were first inoculated into a M9 medium that contained 0.5 g/l NH_4Cl. When IPTG was added into the medium to induce the protein, the ^{15}N-labeled amino (0.1 g/L) and 19 unlabeled amino acids (0.1 g/l) were added at the same time [19]. Protein was then purified as aforementioned for acquiring a ^1H-^{15}N-HSQC spectrum. To prepare an NMR sample, imidazole was removed by using a PD10 column or gel filtration chromatography. Sample was concentrated and put into an NMR tube for data acquisition.

2.3. Gel filtration experiment

Purified protein using Ni^{2+}-NTA resin was concentrated and loaded on a superdex™ 200 10/300 GL column that was pre-equilibrated with a gel filtration buffer (20 mM sodium phosphate, 8 mM dodecylphosphocholine (DPC) and 1 mM DTT). The flow rate was 0.5 ml/min and experiment was conducted at room temperature. The absorbance at 280 nm was monitored continuously and fractions were collected for analysis.

2.4. NMR experiments

NMR samples (0.3 mM) were prepared in 20 mM sodium phosphate buffer, pH 6.5, 1 mM DTT and (100–200 mM) detergent. All NMR spectra were recorded at 313 K on Bruker Avance 600 and Avance 700 spectrometers with cryogenic triple resonance probes [22]. All the pulse programs were from Topspin 2.1 program library. Data were processed with NMRPipe [23] and analyzed using NMRView [24]. Backbone resonances assignment was obtained using 2D-^1H-^{15}N-HSQC, 3D HNCACB, HNCA, HN(CO)CA, HN(CO)CACB, HNCO and HBHACONH experiments. Secondary structure was identified by analysis of ^{13}C secondary chemical shift [25] and TALOS +[26]. Distance constraints were collected from a 3D ^{15}N-edited NOESY (mixing time = 100 ms) experiment using a ^{13}C and ^{15}N-labeled sample under aforementioned conditions. Paramagnetic relaxation enhancement (PRE) experiment was conducted using ^{15}N-labeled samples. $IR_{940-988}$ was prepared at 0.3 mM concentration in the buffer containing 20 mM sodium phosphate, pH6.5, 1 mM DTT, and 120 mM DPC. The 16-doxyl stearic acid (16DSA) was dissolved in d4-methanol to make a 50 mM stock solution. The ^1H-^{15}N-HSQC spectra of $IR_{940-988}$ in the absence and presence of different concentrations of 16DSA were collected. The peak intensities were obtained using NMRview [24]. The ratio of peak intensities before and after adding 16DSA was plotted against residue number.

2.5. Structure determination

The backbone dihedral angle restraints were generated using TALOS +[26]. The NOEs peaks were picked manually and calibrated using NMRview [24]. The nuclear Overhauser effect (NOEs) peak intensity was converted to distance restraints. H–D exchange experiment was conducted by adding D_2O into lyophilized IR in DPC micelles. ^1H-^{15}N-HSQC was recorded immediately when the sample was dissolved in D_2O. The peaks appeared in the HSQC spectrum were used as hydrogen bond restraints. The upper and lower distances used in hydrogen bond restraints were 2.8 and 1.8 Å, respectively. Structure determination was carried out using XPLORE-NIH [27–29]. Structure determination was carried out using a randomized template. Simulated annealing was performed and energy minimization was carried out as previously described [30]. Simulated annealing was carried out with starting temperature of 3000 K and 50, 000 cooling steps. The structure was energy-minimized with 250 steps of Powell energy minimization. Fifty structures were obtained and twenty of them with lowest energies were selected and deposited in protein data bank with access number 2MFR.

2.6. Relaxation analysis

T_1, T_2 and {^1H}-^{15}N steady-state NOE experiments [31] were measured at 313 K using a ^{15}N-labeled sample on a Bruker Avance II 600 MHz spectrometer. For T_1 measurement, the relaxation delays of 5, 40, 80, 130, 330, 470, 630, 800, 900, 1000, 1200, 1400, 1600 and 1800 ms were recorded. For T_2 measurement, the data were acquired with delays of 16.9, 34, 51, 68, 85, 102, 119, 136 and 153 ms. Steady-state {^1H}-^{15}N NOEs were obtained using two datasets that were collected with and without initial proton saturation for a period of 3 s [32].

2.7. Cross-linking experiment

Cross-linking of IR$_{940–988}$ by glutaraldehyde was carried out to test if the purified protein could form a dimer or oligomers in DPC micelles. The method was same as described [33] with some changes in the buffer conditions. Purified samples from *E. coli* were buffer-exchanged to the cross-linking buffer that contained 20 mM Sodium phosphate, pH6.5, 14 mM DPC and 0.1 mM DTT. Protein concentration was diluted to 25 µM to a final volume of 50 µl. Glutaraldehyde (GA) from a 25% stock was added to 16 mM. Mixture was kept at room temperature for 10 min with rotation. Samples with and without cross-linking were separated by SDS-PAGE and protein bands were visualized by Coomassie staining and Western blot using an anti-his antibody.

3. Results

3.1. NMR spectra of IR$_{940–988}$ in detergent micelles

To understand the structure of the TMD of the IR, we expressed and purified a construct that encompasses residues 940 to 988 (IR$_{940–988}$). IR$_{940–988}$ was expressed into inclusion bodies and purified by on-column refolding into different detergent micelles that are necessary for the folding of the TMD. Protein was further purified by gel filtration chromatography (Fig. 2). Detergent micelles have been used for structural study of membrane proteins due to its similarity to cell membrane and small size [34,35]. It is still difficult to decide which detergent is suitable for structural studies without experimental evidence. To select a suitable detergent for structural study, we tested four detergents including Sodium dodecyl sulfate (SDS), DPC, lauryldimethyl amine oxide (LDAO) and lyso-myristoyl phosphatidylglycerol (LMPG) because they were commonly used in membrane protein structural studies by NMR [36–38]. The yield of IR$_{940–988}$ was observed to be similar when these four detergents were used in purification. We could obtain about 0.3 mg of ^{13}C/^{15}N-labeled protein from 1 l culture. The effect of different detergents on the ^{1}H-^{15}N-HSQC spectra was compared (Fig. 3). Purified IR$_{940–988}$ exhibited dispersed cross-peaks in the ^{1}H-^{15}N-HSQC spectra when it was reconstituted into these detergent micelles (Fig. 3). When the construct was reconstituted in LMPG micelles, the ^{1}H-^{15}N-HSQC spectrum showed some broaden peaks, which may arise from the fact that the sample as not homogenous or the presence of multiple

conformations and oligomers when it was purified in LMPG. Among these four detergents, we finally choose DPC micelles for further structural studies because the number of the cross-peaks in the HSQC spectrum agrees well with the residue number of the construct used in this study.

3.2. Secondary structure of IR$_{940–988}$

The resonance assignment of IR$_{940–988}$ in DPC micelles was conducted using conventional 3D experiments. Ambiguities in the assignment were cleared using amino-acid specific labeled samples including ^{15}N-labeled Arg, Phe and Ile. Nearly complete backbone resonances including H(N), N, CO, Cα and Hα and partial side chain resonances including C$_{\beta}$ and H$_{\beta}$ were obtained and the chemical shifts have been deposited in the BioMagResBank (BMRB) with access number 19568. The assignment of ^{1}H-^{15}N-HSQC spectrum is shown in Fig. 4A. Chemical shift analysis using Cα chemical shifts and TALOS + analysis showed that the transmembrane region of the IR is mainly α-helical with a break present (Fig. 4). TALOS + analysis indicated that the break occurs at Gly960. It is not surprising to observe such a kink structure present in the TMD due to the presence of Pro961 (Fig. 4). The C-terminus of IR$_{940–988}$ is disordered. TALOS + and NOE connection analysis shows that there is one short sequence (residues 942–946) that precedes the TMD had a propensity to form a short helix (Fig. 4).

3.3. Solution structure of IR$_{940–988}$

The solution structure of IR$_{940–988}$ in DPC micelles at 313 K was determined using restraints that contained dihedral angles derived from TALOS + and short-range NOEs using Xplor-NIH. The TMD of the IR contains a well-defined α-helix (residues 962 to 976) with a kink containing Gly960 and Pro961 as observed in the secondary structure analysis. The C-terminus region (residues 983–988) following the TMD is flexible. The ensemble of twenty structures of IR$_{940–988}$ with lowest energies is shown in Fig. 5. Table 1 shows the statistics of the determined IR$_{940–988}$ structure. The pair wise root mean squared deviation (rmsd) of the TMD was 0.55 Å for backbone atoms and 1.12 Å for the heavy atoms. As there is no long-range NOE included in structural determination, the orientation of the sequence preceding the TMD was not defined. Surface charge representation of IR$_{940–988}$ showed that TMD
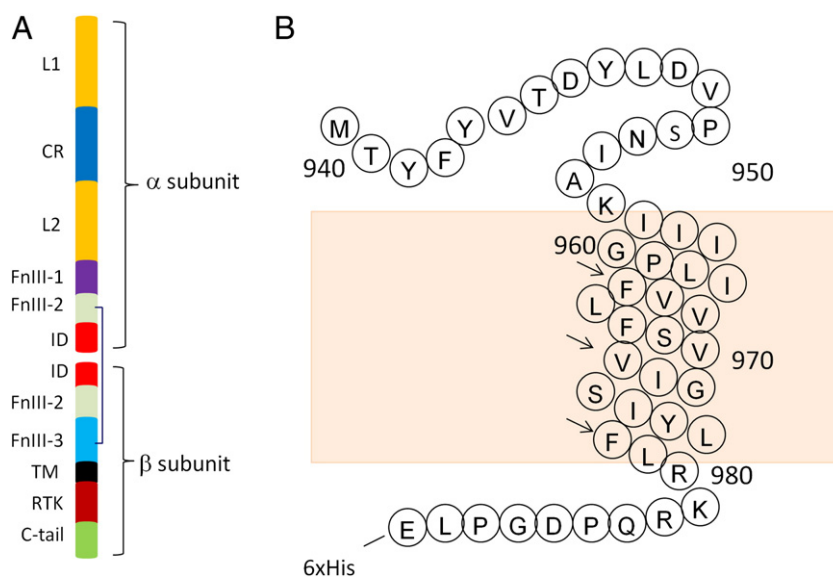

Fig. 1. Insulin receptor and the construct used in this study. A. Insulin receptor diagram. L1, L2, first and second leucine rich repeat; CR, Cys rich domain; FnIII-1-3, fibronectin type III domains 1–3; RTK, receptor tyrosin kinase domain; TM, transmembrane domain; ID, insert domain; C-tail, region after the RKT. B. IR$_{940–988}$ sequence and predicted TMD. Sequence number is based on the sequence from the protein knowledgebase (www.uniprot.org) with access number P06213.
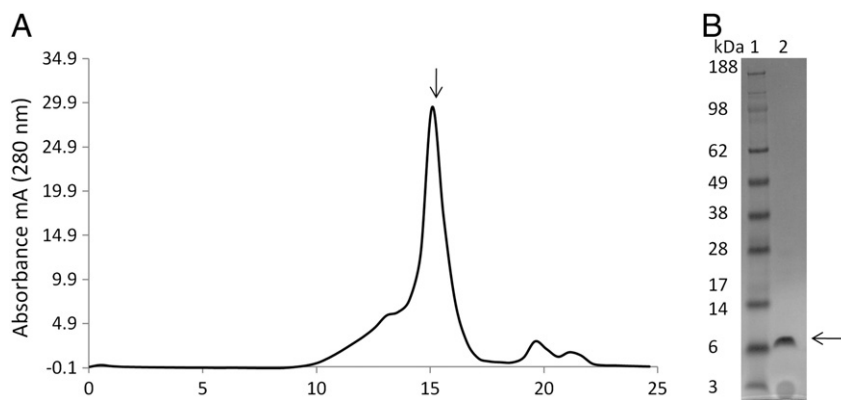
Fig. 2. Purification of IR$_{940-988}$ from *E. coli*. A. Gel filtration profile of IR$_{940-988}$ in DPC micelles. B. SDS-PAGE gel analysis of the purified sample. Protein was expressed and purified as described in Materials and method. 1. Protein molecular weight standard. 2. Purified IR$_{940-988}$. Arrow indicates IR$_{940-988}$.

of the IR was mainly hydrophobic, which is a common feature for a TM region because it contains mainly hydrophobic residues. The residues following the TMD form a positively charged surface which arises from the presence of the charged residues such as Arg (Fig. 1 and 5). The amino acid sequence (residues 942–948) preceding the TMD have a tendency to be a helix based on the TALOS + analysis and the model shows a hydrophobic surface (Fig. 5). Most of the residues forming this helix are hydrophobic (Fig. 5E), suggesting that this modeled

helix may interact with micelles as shown in the model (Fig. 6A). There was no water proton and amide proton NOEs observed for these residues of the region except that residues Thr945 and Asp946 show weak NOEs with water (Fig. 6B). To further probe if the N-terminal amino acids of the TMD interact with micelles, we carried out PRE experiment using 16DSA. If a residue is buried in a micelle or interacts with a micelle, peak intensity will be affected when 16DSA is added [39]. The most affected residues are those compassing residues
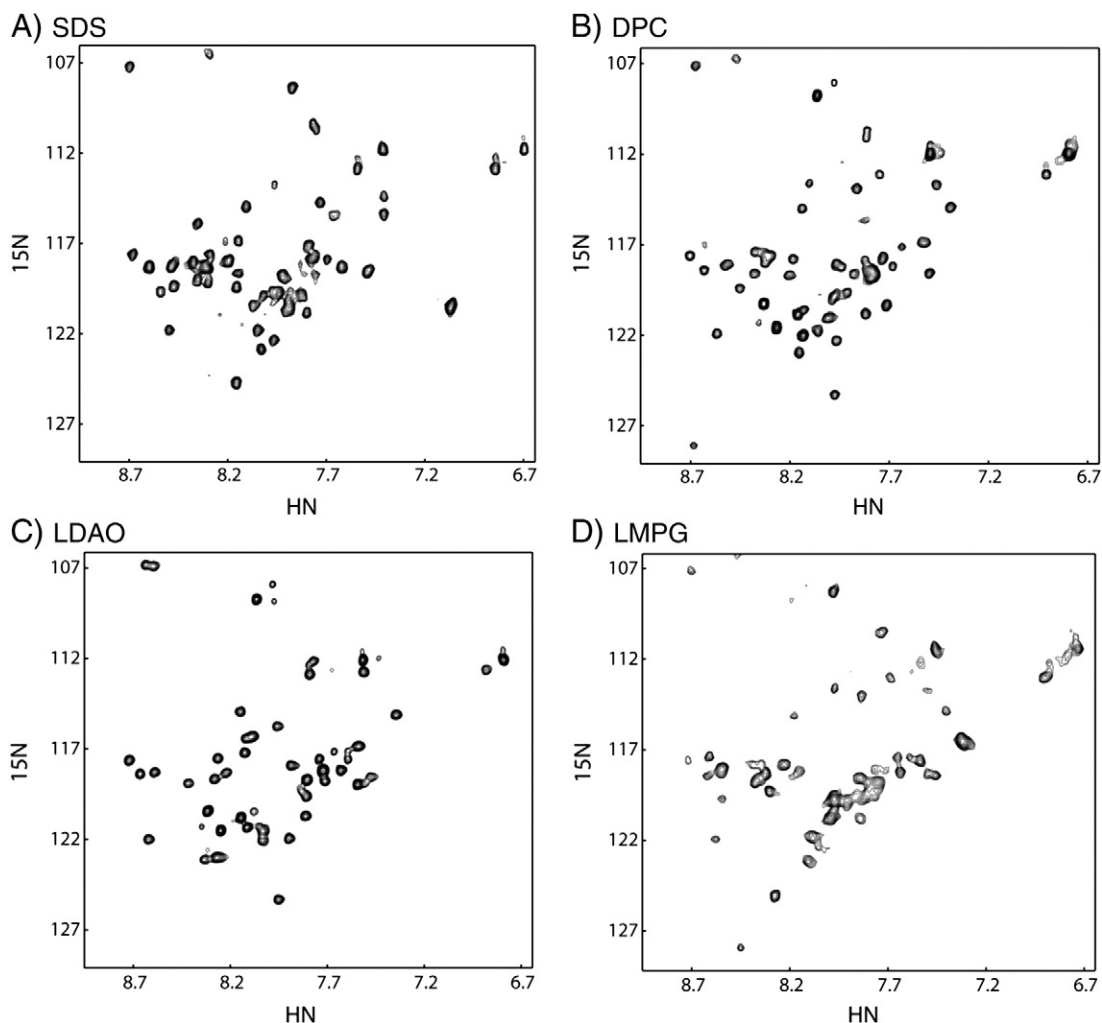

Fig. 3. 2D ^{1}H-^{15}N-HSQC spectra of purified IR$_{940-988}$ in different detergent micelles. All the spectra were acquired at 40 °C. Purified protein (0.3 mM) is in the following detergents: 140 mM SDS (A), 280 mM DPC (B), 200 mM LDAO (C) and 100 mM LMPG (D).
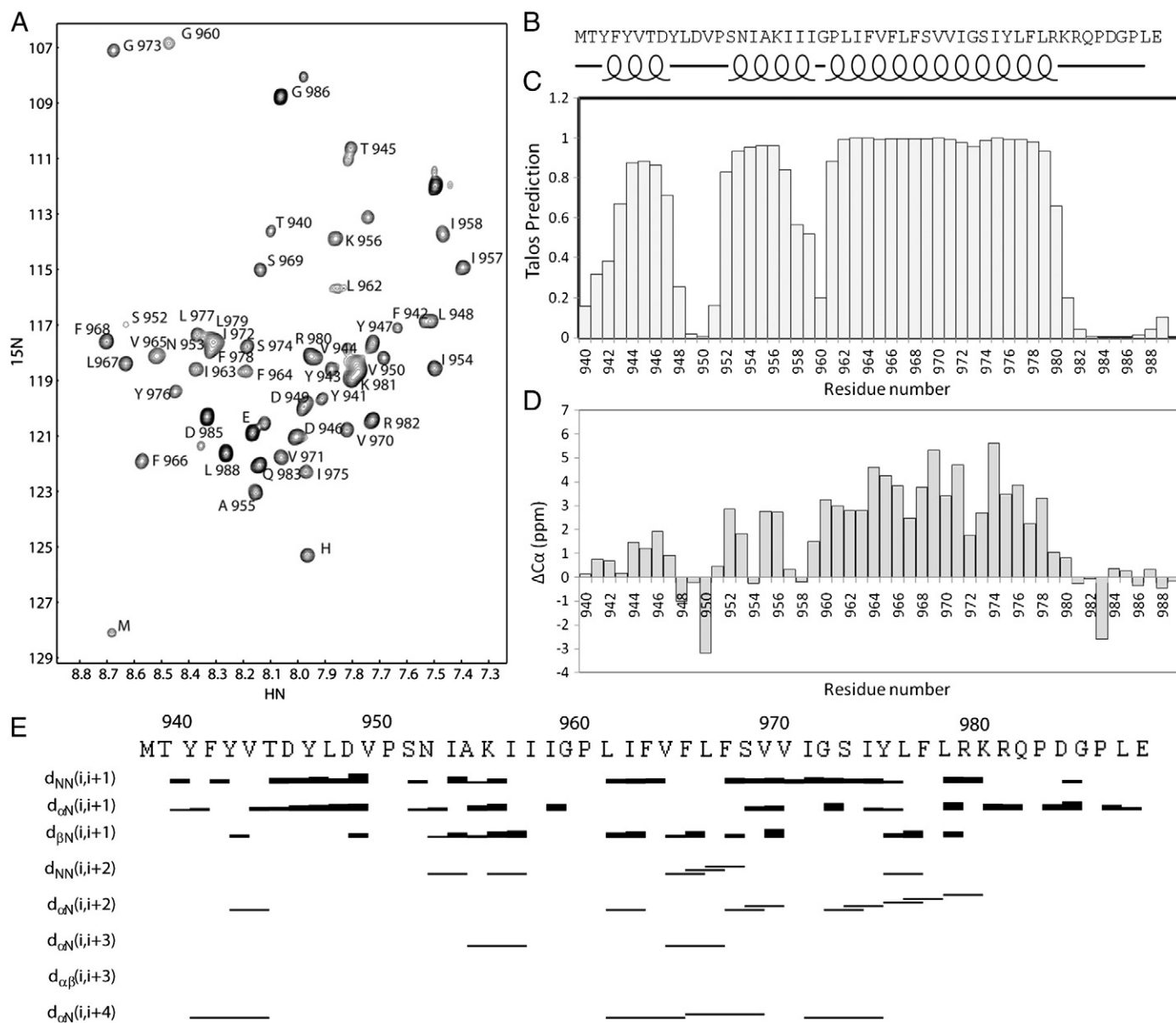
Fig. 4. Assignment of IR$_{940-988}$ in DPC micelles. A. Assignment of the ^{1}H-^{15}N-HSQC spectrum of IR$_{940-988}$ in DPC micelles. B. Amino acid sequence for IR$_{940-988}$ used in the study. The histidine tag was not shown for clarity. C. Secondary structure analysis using TALOS +. The result was obtained from TALOS + analysis [26]. Positive values indicate the possibility (from 0 to 1) to be helical structures, while negative values indicate the possibility to be β-sheets. D. Secondary structure prediction using Cα chemical shifts. The chemical shift differences (ΔCα) between Cα chemical shifts and the random coil values as a function of residue numbers are plotted. Positive value of an amino acid suggests that this residue is helical. E. NOE connections of IR$_{940-988}$ in DPC micelles.

Ile958 to Leu979 that form the TMD of the IR. Some residues from the N-terminal helix are also affected by 16DSA, suggesting that they are buried in or interact with micelles (Fig. 6C). The peak intensities of the residues from the C-terminus and the loop show no significant changes, suggesting that these residues are exposed to the aqueous solution (Fig. 6C). The PRE result and the NOE analysis suggest that the N-terminal amino acid sequence (942–945) is interacting with DPC micelles, which demonstrates that it may interact with cell membrane in vivo.

3.4. Relaxation analysis

The ^{15}N T_1, T_2 and steady-state ^{1}H-^{15}N NOE parameters were measured and analyzed, which is shown in Fig. 7. The N- and C-terminus of IR$_{940-988}$ are flexible, characterized by low T_1, NOE values and higher T_2 values (Fig. 7). The N-terminal region of IR$_{940-988}$ and the TMD of the IR showed different average T_1, T_2 and NOEs, indicating that these two regions existed in different environment. For the TMD, the average T_1 and T_2 values are 0.95 s and 54.2 ms, respectively. For the amino acids (942–948) preceding the TMD, the average T_1 and T_2 values are 0.66 s and 96 ms, respectively. The result suggests that this N-terminal sequence is not completely buried in the micelles. From the T_1/T_2 ratio plateau of the TMD, the overall correlation time for the TMD-DPC micelle complex is roughly 13.0 ns, which is consistent with a protein–DPC micelles aggregate molecular mass in the range of 20–25 kDa. From the relaxation analysis, the residues from Ile957 to Leu980 are buried in the DPC micelles because they have higher T_1 values than that of the average value of the IR$_{940-988}$.

3.5. Cross-linking study

The dynamic studies suggested that IR$_{940-988}$ existed as a monomer in DPC micelles. The oligomeric state of IR$_{940-988}$ was examined when it was diluted in DPC micelles. Chemical cross-linking was carried out
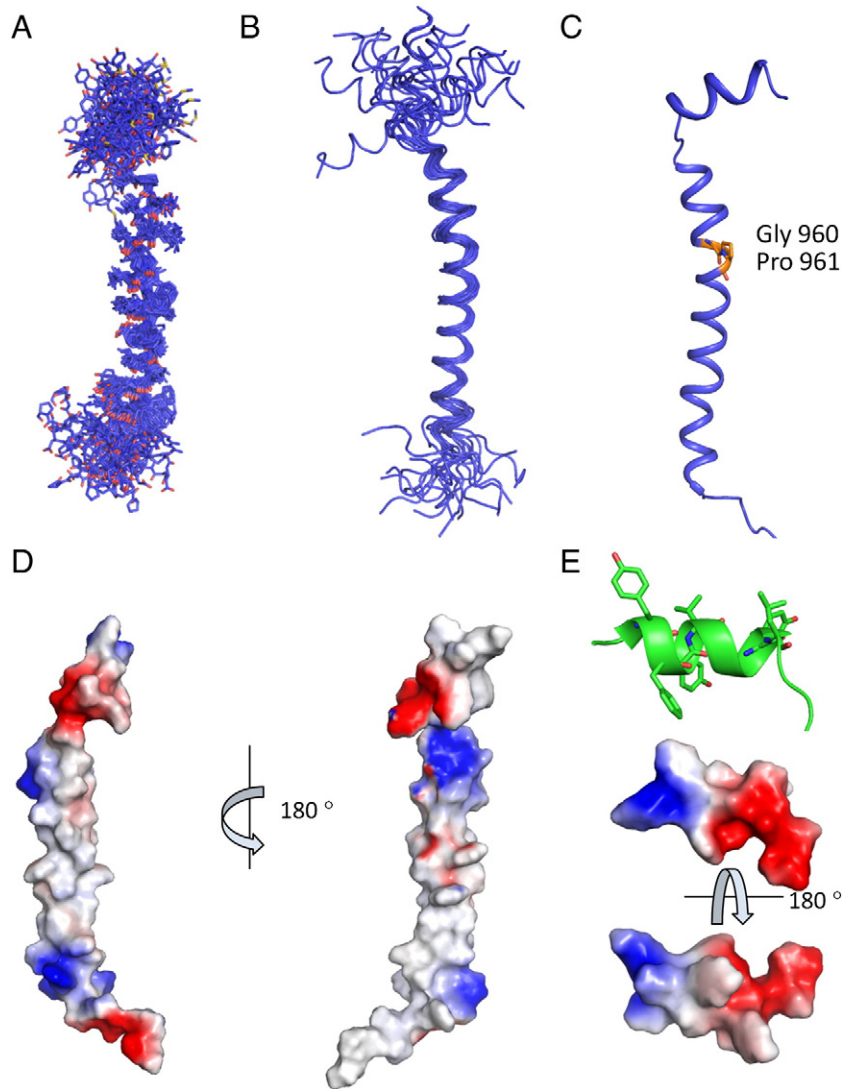
Fig. 5. Structure of $IR_{940-988}$ in DPC micelles. A and B. Superimposed 20 structures with lowest energies. Structures with side chains (A) and only backbone atoms (B) are shown. C. Ribbon representation for the lowest-energy conformer of $IR_{940-988}$. The C-terminal histidine tag is not shown for clarity. Gly and proline residues are shown in sticks. D. Color-coded electrostatic surface potential for the $IR_{940-988}$. All the figures are generated using PyMOL (www.pymol.org). Positive and negative potential are shown in blue and red, respectively. E. Model of the sequence preceding the TMD. The N-terminal sequence was predicted to be a short helix based on dihedral angles derived from TALOS+. The hydrophobic residues are shown in sticks. Upper panel is the cartoon representation of the helix. Middle and bottom panels are color-coded electrostatic surface potential analysis for this helix.

using glutaraldehyde (GA) as a cross-linking reagent. In a SDS-PAGE gel, a dimer band appeared when GA was present, suggesting that this construct could form a dimer under micelle conditions (Fig. 8A). Western blot analysis using an anti-his antibody shows that there are multibands present when GA was added into the protein solution, but the dominant monomer was still present (Fig. 8B). Even after overnight cross-linking with GA, the IR monomer band was still prominent (data not shown). This result suggests that $IR_{940-988}$ could form dimers or trimers under micelle conditions with low affinities.

4. Discussion

In this study, we purified $IR_{940-988}$ of the insulin receptor into DPC micelles and determined its structure using NMR spectroscopy. There is a proline residue present in the TMD and our structural studies suggest that there is a kink present when $IR_{940-988}$ was prepared in DPC micelles. Single-pass membrane proteins with kinked structures present in their TMDs have been observed for several proteins such as KCNE1-a regulator of voltage-gated potassium channels [21] and ost4-a subunit of oligosaccharyltransferase [40,41]. Previous study suggested that vertical motions of the TMD of the IR may not occur during insulin-

stimulated signaling [18]. It is possible that under certain conditions rotation of the TMD helix is a mechanism to transfer the conformational changes caused by insulin binding to the cytoplasmic domain to the kinase domain because rotation of the C-terminal end of the TMD can bring kinase domains in a close contact. The presence of a kink in the TMD might provide the flexibility to alter the orientation of the C-terminal part when insulin binds the IR.

The construct $IR_{940-988}$ used in current study existed mainly as a monomer. As shown in Fig. 2A, the majority of the purified protein had a retention volume of 15 ml, corresponding to a water soluble protein with a molecular weight of 30 kDa. Although we could not use water soluble molecular weight standard to determine the molecular weight of a membrane protein in micelles using gel filtration chromatography, the retention volume of the current construct in micelles suggested that the protein/micelle complex behaves like a large molecular weight protein, which may arise from the presence of detergent micelles. The gel filtration result at least suggests that we are using a homogenous sample in current studies. In the ^1H-^{15}N-HSQC spectrum, $IR_{940-988}$ in DPC micelles exhibited nicely dispersed cross-peaks with narrow line widths, suggesting that the construct exists as a monomer (Fig. 3). Further relaxation data show that protein/micelle complex

Table 1
Summary of the 20 structures of IR$_{940-988}$ in DPC micelles.

Number of unambiguous NOEs	
Intraresidual ($|i - j| = 0$)	24
Short range ($|i - j| \leq 1$)	85
Medium-range ($2 \leq |i - j| < 5$)	22
Long-range ($|i - j| > 5$)	0
Number of dihedral angle constraints	86
Number of hydrogen-bond restraints	32
Number of restraint violations[a]	
Total number of restraint violations > 0.5 Å	0
Total number of dihedral angle constraints > 5°	0
Ramachandran plot statistics[b] *(%)*	
Residues in most favored regions	92.7
Residues in additionally allowed regions	7.3
Residues in generously allowed regions	0
Residues in disallowed regions	0
Average RMSD to mean (Å)	
Backbone (residues 953–981)	0.55 ± 0.15 Å
Heavy atoms (residues 953–981)	1.12 ± 0.20 Å

[a] There are no distance violations greater than 0.5 Å or dihedral angle violations greater than 5°. All residues are included in the final ensemble.

[b] The Ramachandran plot analysis does not include residues (LEHHHHH) at the C-terminus.

may have a molecular weight of 20 kDa corresponding to that of IR$_{940-988}$ peptide and DPC micelles, supporting the conclusion that IR$_{940-988}$ exists as a monomer under current experimental conditions. Previous studies showed that the TMD of the IR may form dimer or oligomer under different condition [15–18]. To test if purified TMD of the IR can form a dimer under micelle conditions, we carried out a GA cross-linking study. Our result demonstrated that the TMD could form a dimer or oligomers, but its binding affinity may be weak (Fig. 8). The reason that we did not obtain a dimer in our current study may be that the ratio between detergent and protein is high, which may affect the formation of TM dimers when the affinity of the TM–TM interaction is low [42]. The appearance of oligomeric band suggested that TMD may have different TM–TM interfaces. In a previous study, replacing the TMD of IR with that of glycophorin A inhibited insulin action [15]. Structural study suggested that TMD of glycophorin A can form strong right-handed dimers even in the presence of SDS micelles [43]. Replacing the TMD with that of c-neu/erbB2 resulted in constitutive kinase activation [18]. The solution structure of the TMD of erbB2 was determined and this domain can form a homo or a hetero dimer with erbB1 under micelle or bicelle conditions [44,45]. The mutagenesis study suggested that the TMD of the IR may form a dimer during insulin signaling. The functional IR TM–TM interaction needs to be weak because the replacing TMD with that of glycophorin A inhibited signaling. There is one SXXXG sequence
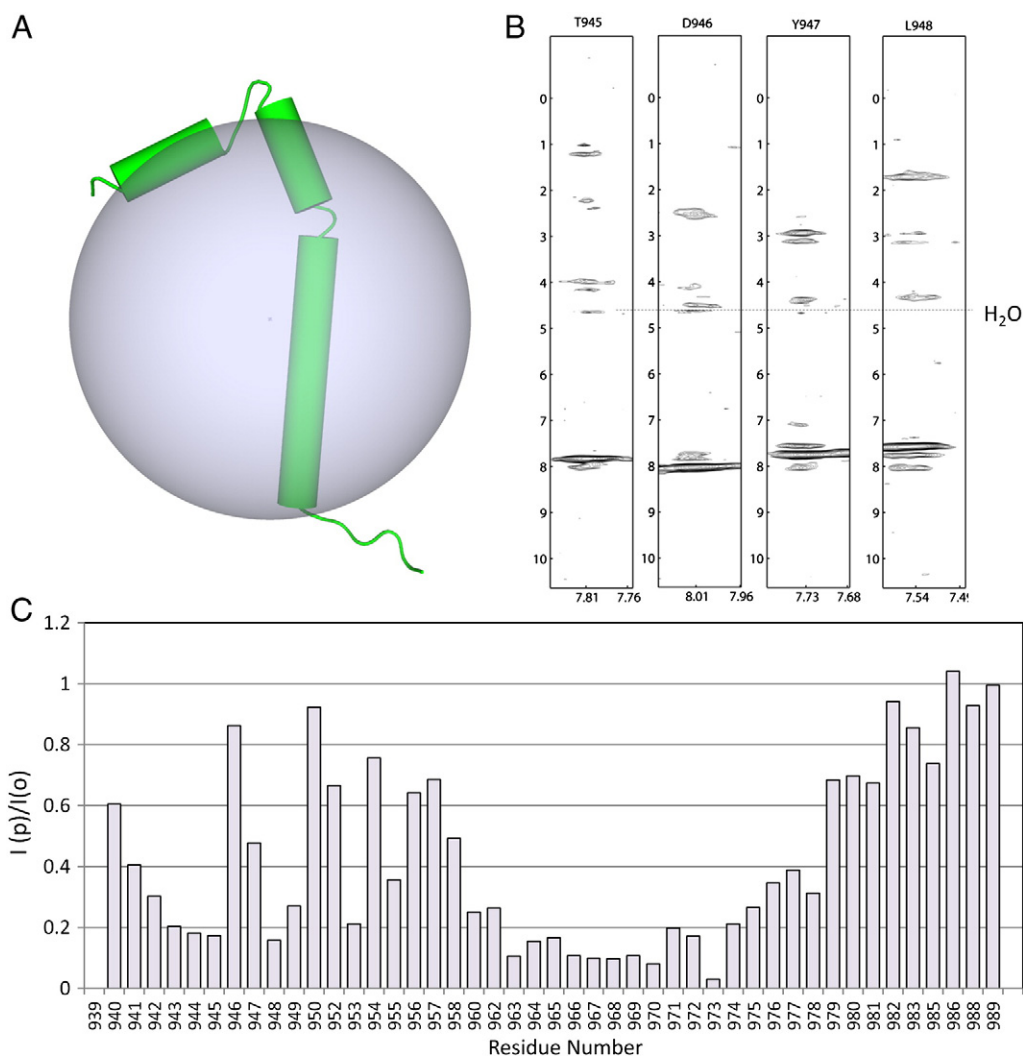

Fig. 6. Model of IR$_{940-988}$ in DPC micelles. A. Model of IR$_{940-988}$. The structure model of IR$_{940-988}$ in DPC micelles was made based on its solution structure. The DPC micelle is drawn as a sphere. B. NOE analysis. The NOEs for some residues from the residues preceding the TMD were plotted from a 3D HSQC-NOESY experiment. The cross peak from water protons is indicated with a dashed line. C. PRE effect of 16DSA on IR$_{940-988}$ in DPC micelles. The relative intensity (I(0)/I(p)) of the cross-peaks in the ^{1}H-^{15}N-HSQC spectra in the absence (I(0)) and presence of 1 mM 16DSA (I(p)) is plotted against residue number.
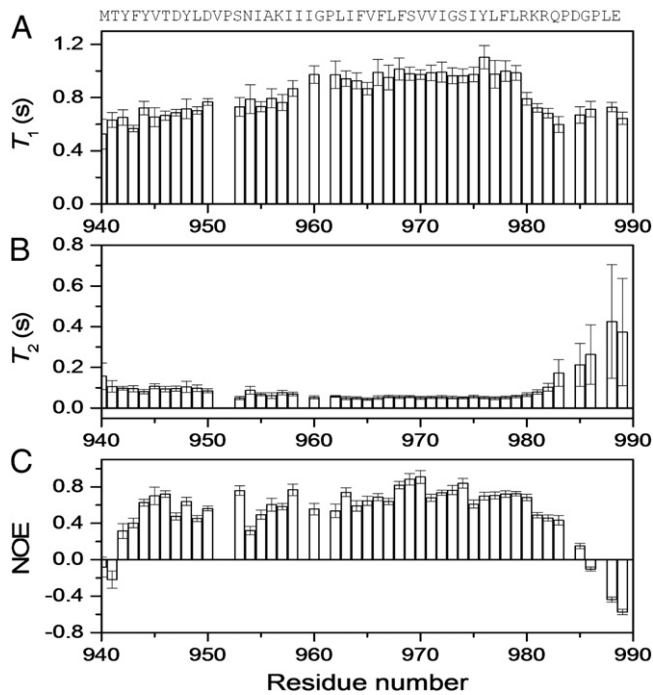
MTYFYVTDYLDVPSNIAKIIIGPLIFVFLFSVVIGSIYLFLRKRQPDGPLE

Fig. 7. NMR relaxation parameters for IR$_{940-988}$ in DPC micelles. All the experiments were recorded at 40 °C. A. T_1 (A), T_2 (B) and {^{1}H}-^{15}N (C) values of the IR940$_{940-988}$ are shown.

present in the TMD of the IR. This sequence may have the function as that of the GXXXG motif that is commonly used in TM–TM packing [46]. This motif might be important for the IR TMD dimerization.

In summary, we purified IR$_{940-988}$ containing the TMD of the IR and reconstituted into DPC micelles. The monomer structure of this construct was determined using NMR spectroscopy. Relaxation and gel filtration chromatography study suggested that the construct exists as a monomer under our experimental conditions. The TMD contains a well-defined helix containing residues 962 to 975. The TMD contains a kink formed by Gly960 and Pro961, which might be important for its function.
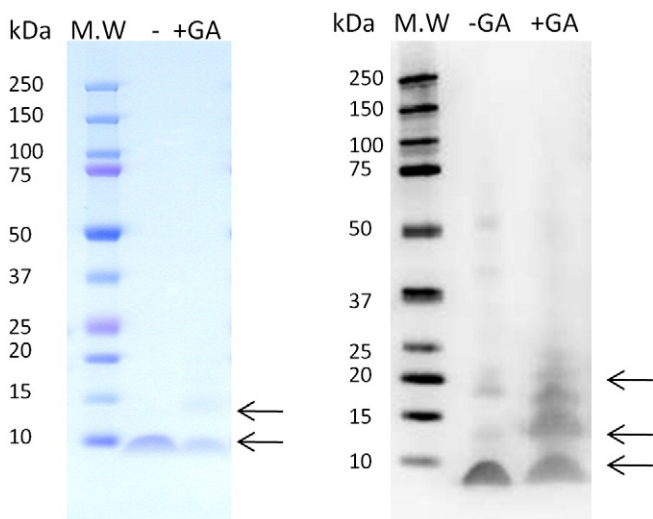

Fig. 8. GA cross-linking of IR$_{940-988}$ in DPC micelles. A. SDS-PAGE of IR$_{940-988}$ before and after cross-linking with GA. B. Western blot analysis of IR$_{940-988}$ before and after cross-linking. The protein was purified in DPC micelles and mixed with GA. The samples without and with GA cross-linking were analyzed by SDS-PAGE followed by Western blot using an anti-his antibody. The protein bands corresponding to IR$_{940-988}$ are indicated with arrows.

References

[1] P. De Meyts, The insulin receptor: a prototype for dimeric, allosteric membrane receptors? Trends Biochem. Sci. 33 (2008) 376–384.
[2] S.R. Hubbard, J.H. Till, Protein tyrosine kinase structure and function, Annu. Rev. Biochem. 69 (2000) 373–398.
[3] M.F. White, C.R. Kahn, The insulin signaling system, J. Biol. Chem. 269 (1994) 1–4.
[4] C.C. Yip, P. Ottensmeyer, Three-dimensional structural interactions of insulin and its receptor, J. Biol. Chem. 278 (2003) 27329–27332.
[5] S.R. Hubbard, The insulin receptor: both a prototypical and atypical receptor tyrosine kinase, Cold Spring Harb. Perspect. Biol. 5 (2013) a008946.
[6] S.R. Hubbard, Structural biology: insulin meets its receptor, Nature 493 (2013) 171–172.
[7] R.Z. Luo, D.R. Beniac, A. Fernandes, C.C. Yip, F.P. Ottensmeyer, Quaternary structure of the insulin–insulin receptor complex, Science 285 (1999) 1077–1080.
[8] V. Copie, Y. Tomita, S.K. Akiyama, S. Aota, K.M. Yamada, R.M. Venable, R.W. Pastor, S. Krueger, D.A. Torchia, Solution structure and dynamics of linked cell attachment modules of mouse fibronectin containing the RGD and synergy regions: comparison with the human fibronectin crystal structure, J. Mol. Biol. 277 (1998) 663–682.
[9] A.E. Whitten, B.J. Smith, J.G. Menting, M.B. Margetts, N.M. McKern, G.O. Lovrecz, T.E. Adams, K. Richards, J.D. Bentley, J. Trewhella, C.W. Ward, M.C. Lawrence, Solution structure of ectodomains of the insulin receptor family: the ectodomain of the type 1 insulin-like growth factor receptor displays asymmetry of ligand binding accompanied by limited conformational change, J. Mol. Biol. 394 (2009) 878–892.
[10] J.G. Menting, J. Whittaker, M.B. Margetts, L.J. Whittaker, G.K. Kong, B.J. Smith, C.J. Watson, L. Zakova, E. Kletvikova, J. Jiracek, S.J. Chan, D.F. Steiner, G.G. Dodson, A.M. Brzozowski, M.A. Weiss, C.W. Ward, M.C. Lawrence, How insulin engages its primary binding site on the insulin receptor, Nature 493 (2013) 241–245.
[11] N.M. McKern, M.C. Lawrence, V.A. Streltsov, M.Z. Lou, T.E. Adams, G.O. Lovrecz, T.C. Elleman, K.M. Richards, J.D. Bentley, P.A. Pilling, P.A. Hoyne, K.A. Cartledge, T.M. Pham, J.L. Lewis, S.E. Sankovich, V. Stoichevska, E. Da Silva, C.P. Robinson, M.J. Frenkel, L.G. Sparrow, R.T. Fernley, V.C. Epa, C.W. Ward, Structure of the insulin receptor ectodomain reveals a folded-over conformation, Nature 443 (2006) 218–221.
[12] B.J. Smith, K. Huang, G. Kong, S.J. Chan, S. Nakagawa, J.G. Menting, S.Q. Hu, J. Whittaker, D.F. Steiner, P.G. Katsoyannis, C.W. Ward, M.A. Weiss, M.C. Lawrence, Structural resolution of a tandem hormone-binding element in the insulin receptor and its implications for design of peptide agonists, Proc. Natl. Acad. Sci. U. S. A. 107 (2010) 6771–6776.
[13] L. Schaffer, A model for insulin binding to the insulin receptor, Eur. J. Biochem. 221 (1994) 1127–1132.
[14] P. De Meyts, Insulin and its receptor: structure, function and evolution, Bioessays 26 (2004) 1351–1362.
[15] A. Gardin, C. Auzan, E. Clauser, T. Malherbe, D. Aunis, G. Cremel, P. Hubert, Substitution of the insulin receptor transmembrane domain with that of glycophorin A inhibits insulin action, FASEB J. 13 (1999) 1347–1357.
[16] J. Whittaker, P. Garcia, G.Q. Yu, D.C. Mynarcik, Transmembrane domain interactions are necessary for negative cooperativity of the insulin receptor, Mol. Endocrinol. 8 (1994) 1521–1527.
[17] S.C. Li, C.M. Deber, S.E. Shoelson, An irregularity in the transmembrane domain helix correlates with the rate of insulin receptor internalization, Biochemistry 33 (1994) 14333–14338.
[18] K. Yamada, E. Goncalves, C.R. Kahn, S.E. Shoelson, Substitution of the insulin receptor transmembrane domain with the c-neu/erbB2 transmembrane domain constitutively activates the insulin receptor kinase in vitro, J. Biol. Chem. 267 (1992) 12452–12461.
[19] Y.M. Kim, S. Gayen, C. Kang, J. Joy, Q. Huang, A.S. Chen, J.L. Wee, M.J. Ang, H.A. Lim, A.W. Hung, R. Li, C.G. Noble, T. Lee le, A. Yip, Q.Y. Wang, C.S. Chia, J. Hill, P.Y. Shi, T.H. Keller, NMR analysis of a novel enzymatically active unlinked dengue NS2B-NS3 protease complex, J. Biol. Chem. 288 (2013) 12891–12900.
[20] Q. Huang, A.S. Chen, Q. Li, C. Kang, Expression, purification, and initial structural characterization of nonstructural protein 2B, an integral membrane protein of Dengue-2 virus, in detergent micelles, Protein Expr. Purif. 80 (2011) 169–175.
[21] C. Kang, C. Tian, F.D. Sonnichsen, J.A. Smith, J. Meiler, A.L. George Jr., C.G. Vanoye, H.J. Kim, C.R. Sanders, Structure of KCNE1 and Implications for How It Modulates the KCNQ1 Potassium Channel, Biochemistry 47 (2008) 7999–8006.
[22] A.S. Chen, Y.M. Kim, S. Gayen, Q. Huang, M. Raida, C. Kang, NMR structural study of the intracellular loop 3 of the serotonin 5-HT(1A) receptor and its interaction with calmodulin, Biochim. Biophys. Acta 1808 (2011) 2224–2232.
[23] F. Delaglio, S. Grzesiek, G.W. Vuister, G. Zhu, J. Pfeifer, A. Bax, NMRPipe: a multidimensional spectral processing system based on UNIX pipes, J. Biomol. NMR 6 (1995) 277–293.
[24] B.A. Johnson, Using NMRView to visualize and analyze the NMR spectra of macromolecules, Methods Mol. Biol. 278 (2004) 313–352.
[25] D.S. Wishart, B.D. Sykes, F.M. Richards, The chemical shift index: a fast and simple method for the assignment of protein secondary structure through NMR spectroscopy, Biochemistry 31 (1992) 1647–1651.

[26] Y. Shen, F. Delaglio, G. Cornilescu, A. Bax, TALOS+: a hybrid method for predicting protein backbone torsion angles from NMR chemical shifts, J. Biomol. NMR 44 (2009) 213–223.

[27] C.D. Schwieters, J.J. Kuszewski, N. Tjandra, G.M. Clore, The Xplor–NIH NMR molecular structure determination package, J. Magn. Reson. 160 (2003) 65–73.

[28] L. Banci, I. Bertini, G. Cavallaro, A. Giachetti, C. Luchinat, G. Parigi, Paramagnetism-based restraints for Xplor–NIH, J. Biomol. NMR 28 (2004) 249–261.

[29] J.J.K. Charles, D. Schwieters, G. Marius Clore, Using Xplor–NIH for NMR molecular structure determination, Prog. Nucl. Magn. Reson. Spectrosc. 48 (2006) 47–2002.

[30] C. Kang, C. Tian, F.D. Sonnichsen, J.A. Smith, J. Meiler, A.L. George Jr., C.G. Vanoye, H.J. Kim, C.R. Sanders, Structure of KCNE1 and implications for how it modulates the KCNQ1 potassium channel, Biochemistry 47 (2008) 7999–8006.

[31] L.E. Kay, D.A. Torchia, A. Bax, Backbone dynamics of proteins as studied by 15 N inverse detected heteronuclear NMR spectroscopy: application to staphylococcal nuclease, Biochemistry 28 (1989) 8972–8979.

[32] S. Gayen, Q. Li, A.S. Chen, T.H. Nguyen, Q. Huang, J. Hill, C. Kang, An NMR study of the N-terminal domain of wild-type hERG and a T65P trafficking deficient hERG mutant, Proteins 79 (2011) 2557–2565.

[33] O. Vinogradova, P. Badola, L. Czerski, F.D. Sonnichsen, C.R. Sanders 2nd, Escherichia coli diacylglycerol kinase: a case study in the application of solution NMR methods to an integral membrane protein, Biophys. J. 72 (1997) 2688–2701.

[34] S. Gayen, Q. Li, C.B. Kang, Solution NMR study of the transmembrane domain of single-span membrane proteins: opportunities and strategies, Curr. Protein Pept. Sci. 13 (2012) 585–600.

[35] C. Kang, Q. Li, Solution NMR study of integral membrane proteins, Curr. Opin. Chem. Biol. 15 (2011) 560–569.

[36] C.R. Sanders, F. Sonnichsen, Solution NMR of membrane proteins: practice and challenges, Magn. Reson. Chem. 44 (2006) S24–S40(Spec No).

[37] M. Etzkorn, T. Raschle, F. Hagn, V. Gelev, A.J. Rice, T. Walz, G. Wagner, Cell-free expressed bacteriorhodopsin in different soluble membrane mimetics: biophysical properties and NMR accessibility, Structure 21 (2013) 394–401.

[38] A. Arora, L.K. Tamm, Biophysical approaches to membrane protein structure determination, Curr. Opin. Struct. Biol. 11 (2001) 540–547.

[39] C. Hilty, G. Wider, C. Fernandez, K. Wuthrich, Membrane protein–lipid interactions in mixed micelles studied by NMR spectroscopy with the use of paramagnetic reagents, Chembiochem 5 (2004) 467–473.

[40] S. Zubkov, W.J. Lennarz, S. Mohanty, Structural basis for the function of a mini membrane protein subunit of yeast oligosaccharyltransferase, Proc. Natl. Acad. Sci. U. S. A. 101 (2004) 3821–3826.

[41] S. Gayen, C. Kang, Solution structure of a human mini membrane protein Ost4, a subunit of the oligosaccharyltransferase complex, Biochem. Biophys. Res. Commun. 409 (2011) 572–576.

[42] T. Zhuang, B.K. Jap, C.R. Sanders, Solution NMR approaches for establishing specificity of weak heterodimerization of membrane proteins, J. Am. Chem. Soc. 133 (2011) 20571–20580.

[43] K.R. MacKenzie, J.H. Prestegard, D.M. Engelman, A transmembrane helix dimer: structure and implications, Science 276 (1997) 131–133.

[44] K.S. Mineev, E.V. Bocharov, Y.E. Pustovalova, O.V. Bocharova, V.V. Chupin, A.S. Arseniev, Spatial structure of the transmembrane domain heterodimer of ErbB1 and ErbB2 receptor tyrosine kinases, J. Mol. Biol. 400 (2010) 231–243.

[45] E.V. Bocharov, K.S. Mineev, P.E. Volynsky, Y.S. Ermolyuk, E.N. Tkach, A.G. Sobol, V.V. Chupin, M.P. Kirpichnikov, R.G. Efremov, A.S. Arseniev, Spatial structure of the dimeric transmembrane domain of the growth factor receptor ErbB2 presumably corresponding to the receptor active state, J. Biol. Chem. 283 (2008) 6950–6956.

[46] D. Schneider, D.M. Engelman, Motifs of two small residues can assist but are not sufficient to mediate transmembrane helix interactions, J. Mol. Biol. 343 (2004) 799–804.